Atmos. Chem. Phys. Discuss., 11, 17879–17911, 2011
www.atmos-chem-phys-discuss.net/11/17879/2011/
doi:10.5194/acpd-11-17879-2011

Atmospheric Chemistry and Physics Discussions

A global climatology of tropospheric and stratospheric ozone derived from Aura OMI and MLS measurements

J. R. Ziemke[1,2], **S. Chandra**[2,3], **G. Labow**[4], **P. K. Bhartia**[2], **L. Froidevaux**[5], and **J. C. Witte**[4]

[1]Goddard Earth and Sciences Technology and Research, Morgan State University, Baltimore, Maryland, USA
[2]NASA Goddard Space Flight Center, Greenbelt, Maryland, USA
[3]Goddard Earth Sciences and Technology, University of Maryland Baltimore County, Baltimore, Maryland, USA
[4]Science Systems and Applications, Inc., Lanham, Maryland, USA
[5]NASA Jet Propulsion Laboratory, Pasadena, California, USA

Received: 23 May 2011 – Accepted: 9 June 2011 – Published: 24 June 2011

Correspondence to: J. R. Ziemke (jerald.r.ziemke@nasa.gov)

Published by Copernicus Publications on behalf of the European Geosciences Union.

Abstract

A global climatology of tropospheric and stratospheric column ozone is derived by combining six years of Aura Ozone Monitoring Instrument (OMI) and Microwave Limb Sounder (MLS) ozone measurements for the period October 2004 through December 2010. The OMI/MLS tropospheric ozone climatology exhibits large temporal and spatial variability which includes ozone accumulation zones in the tropical south Atlantic year-round and in the subtropical Mediterranean/Asia region in summer months. High levels of tropospheric ozone in the Northern Hemisphere also persist in mid-latitudes over the Eastern North American and Asian continents extending eastward over the Pacific Ocean. For stratospheric ozone climatology from MLS, largest ozone abundance lies in the Northern Hemisphere in the latitude range 70° N–80° N in February–April and in the Southern Hemisphere around 40° S–50° S during months August–October. The largest stratospheric ozone abundances in the Northern Hemisphere lie over North America and Eastern Asia extending eastward across the Pacific Ocean and in the Southern Hemisphere south of Australia extending eastward across the dateline. With the advent of many newly developing 3-D chemistry and transport models it is advantageous to have such a dataset for evaluating the performance of the models in relation to dynamical and photochemical processes controlling the ozone distributions in the troposphere and stratosphere. The OMI/MLS ozone gridded climatology data, both calculated mean values and RMS uncertainties are made available to the science community via the NASA total ozone mapping spectrometer (TOMS) website http://toms.gsfc.nasa.gov.

1 Introduction

In a previous paper Ziemke et al. (2006) combined ozone measurements from the Ozone Monitoring Instrument (OMI) and Microwave Limb Sounder (MLS) onboard the Aura satellite to obtain global maps of tropospheric column ozone (TCO). The

ACPD
11, 17879–17911, 2011

derivation of TCO was based upon a tropospheric ozone residual (TOR) method which involved subtracting MLS stratospheric column ozone (SCO) from OMI total column ozone after adjusting for calibration differences between the two instruments. The TOR concept, which was first applied by Fishman et al. (1990) involved measurements of total and stratospheric column ozone from two separate instruments on two separate satellites. Total column ozone was obtained from the Nimbus 7 TOMS UV backscatter instrument while SCO was obtained from Stratospheric Aerosols and Gas Experiment (SAGE) occultation instrument. Aside from calibration issues involving the use of two different satellite measurements, there was also a serious constraint in producing global data with adequate temporal and spatial coverage. Although TOMS total column ozone was daily with near global coverage, SAGE daily SCO measurements were limited to ∼30 ozone profiles per day with about one month required to cover the latitude range 50° S–50° N. Chandra et al. (2003) later combined total column ozone from Nimbus 7 and Earth Probe TOMS with Upper Atmosphere Research Satellite (UARS) MLS ozone measurements to derive improved measurements of TCO extending from the tropics to the extra-tropics; that study was the first to use MLS ozone measurements to derive a long record of TCO spanning ∼6 yr. Having essentially coincident measurements along each orbital track with current Aura OMI and MLS column ozone is a significant improvement from these previous studies in the ability to produce global maps of TCO from daily to longer timescales.

The study by Ziemke et al. (2006) used 2-D interpolation of MLS to derive fields of SCO prior to deriving TCO. This method involved first applying a moving Gaussian interpolation to fill in missing MLS measurements along each daytime orbital track (on average about 14.6 south-to-north orbital tracks per day) followed by linear interpolation along longitude. This simple interpolation scheme for deriving daily gridded SCO fields works well provided that horizontal gradients in SCO are small. Meaningful daily maps of SCO can be determined from 2-D interpolation excluding regions of polar night and the tropospheric wind jets. Other methods have been introduced for obtaining daily maps of SCO and TCO. Schoeberl et al. (2007) introduced a wind trajectory scheme

ACPD
11, 17879–17911, 2011

using MLS ozone profiles and showed improvements for daily SCO and TCO in the extra-tropics. More recently Liu et al. (2010) describes an OMI-only ozone profile retrieval algorithm to derive daily fields of TCO and SCO. Other methods include data assimilation such as from the NASA Global Modeling and Assimilation Office (GMAO) (Stajner, et al., 2008) and also Aura TES ozone profile measurements (Zhang et al., 2010).

All of these methods including simple 2-D interpolation appear to do well in deriving global SCO and TCO for monthly averages, but accurate daily measurements remain generally constrained to excluding the wind jet regions. Even for regions where SCO does not vary appreciably, it remains to be shown that invoking more sophisticated methods beyond simple interpolation are an improvement because of potential induction of additional sources of error such as from assimilated wind fields or other ancillary data input to the algorithm. Tan et al. (2004) have shown that assimilated winds in the stratosphere have substantial errors caused by over-determination of mixing and entrainment rates in subtropical latitudes. Because of this, for a relatively long-lived constituent such as ozone in the lower stratosphere these errors propagate to errors in the tropical SCO field. It remains to be shown which of the various methods can provide adequate accuracy and precision of SCO and TCO in the dynamical wind jet regions to derive true daily global maps (this is current collaborative work in progress).

The objective of this study is to develop a six-year global climatology of TCO and SCO from Aura OMI and MLS measurements. The importance of such a dataset is two-fold: (1) The dataset is useful as a benchmark test of basic seasonal-cycle and seasonal spatial variability present in photochemistry-transport models of tropospheric and stratospheric ozone, and also evaluating ozone precursors, and (2) the OMI/MLS dataset is also potentially useful as a priori information for ozone retrieval algorithms. It is noted that Martin et al. (2007) included an earlier version of OMI/MLS monthly mean TCO and derived an optimal assessment of global tropospheric nitrogen in the Goddard Earth Observing System Chemistry-transport model (GEOS-Chem) which was consistent with both the OMI/MLS ozone and the generated modeled ozone. In other

ACPD
11, 17879–17911, 2011

words, by varying nitrogen in the model it was possible to yield consistent TCO between measurement and model, thus improving confidence in the assessed modeled nitrogen.

In the following, Sect. 2 discusses the OMI and MLS satellite measurements, Sect. 3 compares the TCO with ozonesondes, Sects. 4 and 5 discusses TCO and SCO climatologies from OMI/MLS, and finally Sect. 6 is a summary.

2 Aura OMI and MLS ozone measurements

OMI and MLS are two out of a total of four instruments onboard the Aura spacecraft which is flown in a sun-synchronous polar orbit at 705 km altitude with a 98.2° inclination. Aura was launched in July 2004 and has been providing data measurements since August 2004 to the present. The spacecraft has an equatorial crossing time of 01:45 p.m. (ascending node) with around 98.8 min per orbit (14.6 orbits per day on average). Schoeberl et al. (2006) provide an overview of the EOS Aura mission and discuss the various measurements from the four Aura instruments.

OMI is a nadir-scanner which at visible (350–500 nm) and UV wavelength channels (UV-1: 270–314 nm; UV-2: 306–380 nm) detects backscattered solar radiance to measure column ozone with near global coverage (aside from polar night latitudes) over the Earth with a resolution of 13 km × 24 km at absolute nadir. Aside from ozone, OMI also measures Optical Centroid Cloud Pressure (OCCP), aerosols, NO_2, SO_2, HCHO, and several other trace gases in the troposphere and stratosphere (Levelt et al., 2006). Measurements of ozone from OMI are determined using the OMTO3 v8.5 algorithm which is an extension of the TOMS v8 algorithm. A description of the TOMS v8 algorithm may be obtained from the TOMS V8 CD DVD, or from the OMI Algorithm Theoretical Basis Document (ATBD) from the TOMS web page http://toms.gsfc.nasa.gov/version8/v8toms_atbd.pdf). One main difference between the TOMS v8 and the OMTO3 v8.5 algorithms is the treatment of clouds. The TOMS v8 and earlier versions of OMTO3 use a cloud pressure climatology based on

ACPD
11, 17879–17911, 2011

thermal infrared cloud-top pressures, whereas OMTO3 v8.5 uses OCCP derived with OMI by the rotational Raman scattering method. The use of simultaneously measured OCCP significantly improves estimates of total column ozone, especially in the presence of bright clouds (Joiner and Vasilkov, 2006). The OMI instrument began having scan measurement errors beginning in year 2007 which are called row anomalies. The OMI instrument has 60 scan rows per orbit path and currently about 1/3 of the scan row measurements are affected. This problem is caused by partial blockage from material in the optical field of OMI but has not degraded appreciably since January 2009.

SCO is calculated for the OMI/MLS residual method using MLS v3.3 ozone profile measurements. The MLS instrument is a thermal-emission microwave limb sounder that measures vertical profiles of mesospheric, stratospheric, and upper tropospheric temperature, ozone, and several other important constituents such as CO and H_2O from limb scans taken in the direction ahead of the Aura satellite orbital track. The MLS profile measurements are made about 7 min before OMI views the same location during ascending (daytime) orbital tracks. These we refer to as "co-located" measurements between OMI and MLS. MLS also measures ozone and other atmospheric constituents for descending nighttime orbits which on a given day can be up to ±12 h different in time from OMI daytime measurements. With combined ascending and descending nodes MLS makes around 3500 vertical profile measurements over the Earth per day. This study includes only the ascending orbit co-located data from MLS for deriving SCO. Details regarding the instrument including spectrometers, spectral channels, calibration, and other topics are discussed by Waters et al. (2006) and in related papers in the same journal. Froidevaux et al. (2008) provides validation results for MLS v2.2 measurements of ozone and other trace gases. At the present time both v2.2 and v3.3 are provided to the science community. While v2.2 retrieval has 37 pressure levels, v3.3 has 55 pressure levels and other improvements; however, v3.3 also has more outliers and missing data in the ozone profile measurements than with v2.2. Our analysis of SCO from MLS shows that there is little difference between using v2.2 or v3.3 other than a small systematic offset (v3.3 minus v2.2) at all latitudes of

ACPD
11, 17879–17911, 2011

about +2.5 DU. As was similarly done by Ziemke et al. (2006), MLS v3.3 SCO was adjusted to CCD SCO from OMI by subtracting this offset from MLS SCO. Information regarding the MLS v3.3 ozone measurements including a data quality description document is available online from the NASA Data and Information Services Center webpage (http://disc.sci.gsfc.nasa.gov/gesNews/mls_new_data_version_release).

For the OMI/MLS residual method SCO is determined from vertically integrated MLS ozone profiles which is subtracted from OMI total column ozone to derive TCO. Tropopause pressure, which separates tropospheric from stratospheric column ozone comes from National Centers for Environmental Prediction (NCEP) using the World Meteorological Organization (WMO) $2\,\mathrm{K\,km^{-1}}$ lapse rate tropopause definition. SCO from MLS is determined by pressure integration of ozone volume mixing ratio profiles from 0.0215 hPa down to the NCEP tropopause. The MLS ozone profile measurements were linearly interpolated in log-pressure to the NCEP tropopause pressure to derive SCO. MLS SCO (in Dobson Units, DU; $1\,\mathrm{DU} = 2.69 \times 10^{20}$ molecules $\mathrm{m^{-2}}$) was determined by standard log-pressure integration of ozone partial pressure: $\mathrm{SCO} = 0.79 \int_{0.0215\ \mathrm{hPa}}^{\mathrm{Ptropopause}} XP \cdot d\ln P$, where X is ozone volume mixing ratio in units ppmv and P is pressure in units hPa. The recommended range for scientific analysis of MLS v3.3 ozone profiles is 0.0215–261 hPa. As was done by Ziemke et al. (2006), nearly global SCO from MLS for each day was achieved by including ozone retrievals down to 316 hPa. The uncertainty in derived SCO from MLS by including the 316 hPa level beyond 261 hPa can be estimated. Documentation for MLS v3.3 ozone measurements suggests RMS uncertainties of about 0.03 ppmv at 261 hPa and 0.05 ppmv at 316 hPa. Using the above integration formula, an upper-bound estimate of the RMS uncertainty in 261–316 hPa column ozone from MLS is then about 3.5 DU.

MLS SCO data were initially binned to 1° latitude × 1.25° longitude to be compatible with OMI level-3 (L3) gridded total column ozone. Tropopause pressures from NCEP analyses were re-binned to this same resolution from a coarser 2.5° × 2.5° gridding. It is noted for MLS limb measurements that the horizontal optical path is about 300 km which is larger than the horizontal size of OMI L3 gridded data, but is comparable to the

ACPD
11, 17879–17911, 2011

size of original NCEP gridded measurements. To derive a high density SCO field we have used the two-step spatial interpolation of Ziemke et al. (2006). The interpolation for SCO includes first a moving 2-D (latitude/longitude) Gaussian window along daytime orbit to fill in intermittent gaps along-track for MLS SCO, followed secondly by a linear interpolation along longitude between MLS SCO data. This interpolation approach preserves the along-track measurements of SCO from MLS at all latitudes. NCEP measurements of tropopause pressure were re-binned to the same 1° latitude × 1.25° longitude resolution. Following derivation of daily maps of SCO and TCO at 1° × 1.25° resolution, the data were averaged monthly in 5° × 5° and 10° × 10° bins. We have evaluated OMI and MLS ozone data for the time period 1 October 2004–31 December 2010 which represents approximately six years of continuous measurements. The TCO and SCO monthly climatology fields were smoothed along longitude using Fourier analysis by retaining zonal wave numbers 0–12 which both reduces noise and ensures periodic continuation across the dateline.

3 Comparisons of OMI/MLS tropospheric ozone with ozonesondes

Validation of OMI/MLS TCO is based upon Southern Hemisphere Additional OZonseondes (SHADOZ) and World Ozone and Ultraviolet radiation Data Center (WOUDC) ozonesonde measurements whereby monthly means from OMI/MLS are compared with monthly ensemble averages from the ozonesondes. The ozonesonde data represent for each station an average of all existing ozonesonde measurements in a given month (which could vary from one to several). OMI/MLS TCO was converted to ozone mean volume mixing ratio and then compared with mean volume mixing ratio for both the SHADOZ and WOUDC ozonesondes. Ozone mean volume mixing ratio for the tropical SHADOZ stations involved pressure averaging of ozone for ground-to-120 hPa while for extra-tropical WOUDC stations this was ground-to-350 hPa. The ozonesonde data for our comparisons extend for years 2004–2009 for SHADOZ and 2005–2008 for WOUDC. Of the several SHADOZ and WOUDC stations processed, 39 of them had

ACPD
11, 17879–17911, 2011

measurements that overlapped with the OMI/MLS time period.

Figures 1 and 2 show tropospheric ozone time series comparisons for several stations from SHADOZ and WOUDC, respectively. Also included in these figures are 1-1 scatter diagrams of the combined data. The stations in Figs. 1 and 2 were chosen not just because these are common stations but also because of large annual-cycle variability (20–30 ppbv peak-to-peak) with nearly complete month-to-month temporal coverage.

There are important issues involved when comparing ozonesondes with satellite ozone measurements. Balloon ozonesondes represent wind advected measurements along trajectory paths and are very different than the satellite measurements which provide ozone averages over broad regions. Also, ozone in the troposphere (such as shown by Avery et al., 2010) exhibits large changes of 30–50 ppbv over horizontal distances of only a few km or less. With such enormous spatial variability the most one can gain in comparing satellite measured ozone versus ozonesondes is to evaluate seasonal variability and climatological means, and extreme cases such as inter-annual variability events in the tropical Pacific caused by ENSO. Table 1 provides a list of comparisons between OMI/MLS and the SHADOZ/WOUDC ozonesondes with station latitudes arranged from northern-most at top to southern-most at bottom. Listed for each station is the total number of daily profile measurements, mean values for OMI/MLS and ozonesondes, and standard RMS of their differences. For most of the stations listed in Table 1 the RMS values lie between 4 ppbv and 10 ppbv. For stations northward of 50° N, RMS is greater than 10 ppbv except for Debilt and Valentia. The larger RMS numbers in NH high latitudes are partly explained by the sparse nature of monthly measurements from both OMI/MLS and ozonesondes. Figure 3 compares climatological means for OMI/MLS and ozonesondes. The left panel in Fig. 3 represents station latitudes 25° S–50° N and the right panel is the same but includes stations poleward of 50° N.

ACPD
11, 17879–17911, 2011

4 Comparisons of OMI/MLS and LLM tropospheric ozone climatology

Logan (1999) provided an extensive analysis of global ozone based upon ozonesonde measurements. More recently McPeters et al. (2007) expanded the ozonesonde evaluation of Logan (1999) and derived a global zonal mean climatology of total atmospheric ozone as a function of latitude, altitude, and month of year. This climatology was determined by combining ozonesondes with satellite ozone measurements from SAGE and MLS. The final climatology product is referred to as the Labow-Logan-McPeters (LLM) climatology and is currently used in the OMTO3 v8.5 algorithm processing for both OMI and TOMS ozone retrievals.

Figure 4 shows a comparison of LLM TCO climatology (top panel) with OMI/MLS TCO climatology (middle panel) and their difference (bottom panel). Fundamental characteristics are generally consistent between the datasets regarding seasonal cycles including the transition in peak TCO in the NH from tropics to mid-latitudes when going from spring to summer months. LLM minus OMI/MLS TCO difference is larger by several DU to more than +5 DU for some months and latitudes in the subtropics and mid-latitudes. These differences are largely explained as an ozonesonde station location issue as the LLM climatology is determined from TCO measurements over land whereas TCO from OMI/MLS in Fig. 4 is averaged along all longitudes.

That is, because TCO over ocean is generally smaller than over land (as discussed later for Fig. 5), OMI/MLS zonal mean TCO will be smaller than LLM TCO. In contrast, in the high latitudes of both hemispheres in Fig. 4 the offset differences are instead negative exceeding −5 DU. These differences in the higher latitudes may be explained by both a sparse number of ozonesonde measurements and also high solar-zenith angles which can produce substantial errors in the OMI and/or MLS ozone retrievals.

ACPD
11, 17879–17911, 2011

5 OMI/MLS global TCO climatology maps

The first study to derive a global TCO climatology maps from satellite measurements was Fishman et al. (1990). As noted in the Introduction, tropospheric ozone determined from TOMS/SAGE residual was limited both temporally and spatially because of sparse SAGE ozone profile measurements. An improvement was made for the SAGE sampling problem by Fishman et al. (2003) by using instead NOAA SBUV to derive SCO, however there is little ozone profile information obtained from SBUV below the ozone number density peak (i.e., atmospheric pressures greater than ∼ 30–40 hPa). To alleviate this SBUV ozone profile problem Fishman et al. (2003) applied an empirical correction to SBUV ozone profiles to improve the SCO fields. It is anticipated that the use of Aura MLS ozone profile measurements which extend down to 261 hPa for v3.3 substantially improves global climatology estimates of SCO and also TCO.

A six-year TCO climatology from OMI and MLS ozone is shown in Fig. 5a–c for each of the months January–December. Figure 5 for illustration plots the $10^{\circ} \times 10^{\circ}$ dataset. TCO in high latitudes is flagged as missing, both for obvious reason involving polar night latitudes (i.e., where there are no OMI measurements) and additional subjective data flagging. Subjective data flagging included OMI scenes with solar zenith angles greater than 82° or questionable derived TCO product values in high latitudes.

The main features of the TCO climatology in Fig. 5 are briefly summarized. In tropical latitudes TCO for each month is characterized by low amounts in the Pacific ∼ 15–20 DU with much higher columns ∼ 35–45 DU in the Atlantic. Lowest TCO in the tropics lies in the Western Pacific in July–September with numbers less than 15 DU. These low columns are largely a manifestation of deep convection and vertical injection of low marine boundary layer/low tropospheric ozone into the middle and upper troposphere. The highest TCO in the tropics occurs in September–October in the Southern Atlantic region extending eastward toward Australia with numbers 40–45 DU. These annually recurring high values in the Southern Hemisphere are associated with planetary-scale transport of ozone rich air mass and ozone sources including effects from STE and

ACPD
11, 17879–17911, 2011

biomass burning. TCO in the Northern Hemisphere has large topographic variability year-round, with largest columns occurring around May–July over the Eastern US eastward over the Atlantic Ocean toward Europe, Mediterranean/Western Asia, and Eastern Asia extending eastward over the Pacific Ocean toward North America.

Figure 6 shows line plots of TCO as a function of longitude for 30°–40° N and 0°–10° S. These latitude bands and months were chosen to show several large annually recurring features present in global TCO. The line plots in Fig. 6 also include $\pm 2\sigma$ uncertainties for illustration where σ is calculated standard RMS error of the mean. TCO in these two latitude bands has large spatial variability. The left panel shows zonal variability caused by a Mediterranean-Asian accumulation region (centered about 30° E) and the mountains of the Tibetan Plateau (centered about 90° E). The right panel shows large contrast in TCO from low values in the tropical Pacific and high values in the tropical Atlantic (i.e., about 20 DU versus 40 DU, respectively). The $5° \times 5°$ and $10° \times 10°$ monthly TCO climatology fields along with their RMS uncertainty fields can be obtained via link from the TOMS webpage (http://toms.gsfc.nasa.gov).

For applications such as evaluating 3-D chemistry-transport models of the atmosphere it is useful to derive a zonal mean climatology of TCO from OMI/MLS. A simple model comparison with zonal mean TCO climatology can reveal fundamental offsets or annual-cycle differences that can be used to aid in the development of models. Ziemke et al. (2006) compared an earlier version of zonal mean TCO between OMI/MLS and the Global Modeling Initiative (GMI) 3-D model and showed good agreement in latitude gradients and temporal variability except for a 5–10 DU offset in the NH extending from the subtropics out to mid-latitudes. It was surmised that errors in OMI from aerosols could be a contributing factor for the offset, but the primarily indication was that the model was over-determining TCO by several DU in the NH subtropics/mid-latitudes in most months. Figure 7 shows the six-year climatology of zonal mean TCO. Lowest TCO occurs in the SH tropics around 10° S around January–April (< 24 DU) and also in the NH and SH mid-latitudes around late fall to winter-spring (< 30 DU). Largest TCO occurs in the NH mid-latitudes in June–July (> 42 DU) and in the SH subtropics

ACPD
11, 17879–17911, 2011

during September–November (> 39 DU). There is a transition in the NH from peak values in spring months (March–May) in the tropics/subtropics to peak values in summer (June–July) in the mid-latitudes. This pattern shift from spring to summer with latitude is caused largely by a coupling of spring-summer STE with ozone produced from pollution events in summer months. It is noted that the GMI model evaluated by Ziemke et al. (2006) showed all the basic temporal and spatial features in Fig. 7 despite an offset difference in the NH mid-latitudes.

6 MLS global SCO climatology maps

An SCO climatology from MLS is shown in Fig. 8a–c for each of the months January–December. As in Fig. 4 the data binning is at $10^{\circ} \times 10^{\circ}$ resolution which for SCO provides nearly global coverage out to central latitudes $\pm 85^{\circ}$. The main features include a contrast between small zonal variability of SCO in the tropics and large planetary-scale variability in the middle and high latitudes in both hemispheres. SCO in Fig. 8 should be interpreted carefully in the middle and high latitudes particular to these years 2004–2010 since SCO patterns in both hemispheres can exhibit substantial inter-annual differences in zonal variability caused by stratospheric sudden warming events and the morphology of the breakup of the middle atmosphere polar vortex in the NH and SH. Zonal mean SCO from MLS is shown in Fig. 9. SCO in Fig. 9 is largest in spring months in both hemispheres. In the Northern Hemisphere SCO is largest around February–March at high latitudes and in the Northern Hemisphere SCO is largest around September–October in mid-latitudes. The maximum SCO in the NH occurs in conjunction with high ozone over the Central Asian continent extending eastward across North America as shown in Fig. 7a. SCO in the SH maximizes equator-ward of the polar vortex in September–October and as Fig. 7c shows, originates primarily from the Pacific about the dateline. Table 3 shows the calculated zonal mean SCO climatology values given in 5° latitude bands.

ACPD
11, 17879–17911, 2011

7 Summary

A six-year global climatology of tropospheric column ozone (TCO) and stratospheric column ozone (SCO) is derived from combining Aura OMI and MLS measurements for the period October 2004–December 2010. The climatology is useful for several purposes including evaluation of 3-D chemistry-transport models and self-generating global circulation models of the atmosphere to assess model performance. By comparing basic seasonal cycles and seasonally-varying spatial variability in TCO and SCO in models with the climatology one can identify and correct problems in models regarding errors in wind fields or invoked photochemical reactions/rates, and errors in emissions including ozone precursors. Another useful application for the global climatology of TCO and SCO includes producing a climatology of radiative forcing coming from upper and lower atmospheric ozone. The total column ozone climatology determined from adding together SCO and clear-sky TCO can also generate a global clear-sky surface UV climatology as a function of region and time of year.

Algorithms for retrieving ozone such as from remote sensing satellite instruments rely on assumed a priori information of the ozone concentrations. The current OMTO3 algorithm invokes the Labow-Logan-McPeters (LLM) zonal mean ozone climatology (McPeters et al., 2007) which is determined by combining ozonesondes with SAGE and Aura MLS ozone profile measurements. The LLM climatology is given as a function of month, latitude, and altitude. A future task is to combine the LLM and the OMI/MLS climatology products to generate a single 3-D (latitude, longitude, altitude) 12-month climatology.

The TCO and SCO climatology data from OMI/MLS are provided to the community in ASCII formatted tables with IDL and Fortran readers as a link from the TOMS homepage (http://toms.gsfc.nasa.gov). The measurements along with their computed RMS uncertainties are given in these tables at $5^\circ \times 5^\circ$ and $10^\circ \times 10^\circ$ (latitude × longitude) resolution.

ACPD
11, 17879–17911, 2011

Acknowledgements. The authors thank the Aura MLS and OMI instrument and algorithm teams for the extensive satellite measurements used in this study. OMI is a Dutch-Finnish contribution to the Aura mission. Funding for this research was provided in part by NASA NNH07ZDA001N-AST.

References

Avery, M., Twohy, C., McCabe, D., Joiner, J., Severance, K., Atlas, E., Blake, D., Bui, T. P., Crounse, J., Dibb, J., Diskin, G., Lawson, P., McGill, M., Rogers, D., Sachse, G., Scheuer, E., Thompson, A. M., Trepte, C., Wennberg, P., and Ziemke, J.: Convective distribution of tropospheric ozone and tracers in the Central American ITCZ region: Evidence from observations during TC4, J. Geophys. Res., 115, D00J21, doi:10.1029/2009JD013450, 2010.

Chandra, S., Ziemke, J. R., and Martin, R. V.: Tropospheric ozone at tropical and middle latitudes derived from TOMS/MLS residual: comparison with a global model, J. Geophys. Res., 108, D9, doi:10.1029/2002JD002912, 2003.

Fishman, J., Watson, C. E., Larsen, J. C., and Logan, J. A.: Distribution of tropospheric ozone determined from satellite data, J. Geophys. Res., 95, 3599–3617, 1990.

Fishman, J., Wozniak, A. E., and Creilson, J. K.: Global distribution of tropospheric ozone from satellite measurements using the empirically corrected tropospheric ozone residual technique: Identification of the regional aspects of air pollution, Atmos. Chem. Phys., 3, 893–907, doi:10.5194/acp-3-893-2003, 2003.

Froidevaux, L., Jiang, Y. B., Lambert, A., Livesey, N. J., Read, W. G., Waters, J. W., Browell, E. V., Hair, J. W., Avery, M. A., McGee, T. J., Twigg, L. W., Sumnicht, G. K., Jucks, K. W., Margitan, J. J., Sen, B., Stachnik, R. A., Toon,G. C., Bernath, P. F., Boone, C. D., Walker, K. A., Filipiak, M. J., Harwood, R. S., Fuller, R. A., Manney, G. L., Schwartz, M. J., Daffer, W. H., Drouin, B. J., Cofield, R. E., Cuddy, D. T., Jarnot, R. F., Knosp, B. W., Perun, V. S., Snyder, W. V., Stek, P. C., Thurstans, R. P., and Wagner, P. A.: Validation of Aura Microwave Limb Sounder stratospheric ozone measurements, J. Geophys. Res., 113, D15S20, doi:10.1029/2007JD008771, 2008.

Joiner, J. and Vasilkov, A. P.: First results from the OMI Rotational Raman Scattering Cloud Pressure Algorithm, IEEE T. Geosci. Remote, 44, 1272–1282, 2006.

Levelt, P. F., Hilsenrath, E., Leppelmeier, G. W., van den Oord, H. J., Bhartia, P. K., Tamminen,

ACPD

11, 17879–17911, 2011

J., de Haan, J. F., and Veefkind, J. P.: Science objectives of the ozone monitoring instrument, IEEE T. Geophys. Remote, 44(5), 1199–1208, 2006.
Liu, X., Bhartia, P. K., Chance, K., Spurr, R. J. D., and Kurosu, T. P.: Ozone profile retrievals from the Ozone Monitoring Instrument, Atmos. Chem. Phys., 10, 2521–2537, doi:10.5194/acp-10-2521-2010, 2010.
Logan, J. A.: An analysis of ozonesonde data for the troposphere: recommendations for testing 3-D models, and development of a gridded climatology for tropospheric ozone, J. Geophys. Res., 104, 16115–16149, 1999.
Martin, R. V., Sauvage, B., Folkins, I., Sioris, C. E., Boone, C., Bernath, P., and Ziemke, J.: Space-based constraints on the production of nitric oxide by lightning, J. Geophys. Res., 112, D09309, doi:10.1029/2006JD007831, 2007.
McPeters, R. D., Labow, G. J., and Logan, J. A.: Ozone climatological profiles for satellite retrieval algorithms, J. Geophys. Res., 112, D05308, doi:10.1029/2005JD006823, 2007.
Schoeberl, M. R., Douglass, A. R., Hilsenrath, E., Bhartia, P. K., Barnett, J., Beer, R., Waters, J., Gunson, M., Froidevaux, L., Gille, J., Levelt, P. F., and DeCola, P.: Overview of the EOS Aura Mission, /IEEE Trans. Geosci. Remote Sens., 44/(5), 1066–1074, May 2006.
Schoeberl, M. R., Ziemke, J. R., Bojkov, B., Livesey, N., Duncan, B., Strahan, S.,Froidevaux, L., Kulawik, S., Bhartia, P. K., Chandra, S., Levelt, P. F., Witte, J. C., Thompson, A. M., Cuevas, E., Redondas, A., Tarasick, D. W., Davies, J., Bodeker, G., Hansen, G., Johnson, B. J., Oltmans, S. J., Vomel, H., Allaart, M., Kelder, H., Newchurch, M., Godin-Beekmann, S., Ancellet, G., Claude, H., Andersen, S. B., Kyro, E., Parrondos, M., Yela, M., Zablocki, G., Moore, D., Dier, H., von der Gathen, P., Viatte, P., Stubi, R., Calpini, B., Skrivankova, P., Dorokhov, V., De Backer, H., Schmidlin, F. J., Coetzee, G., Fujiwara, M., Thouret, V., Posny, F., Morris, G., Merrill, J., Leong, C. P., Koenig-Langlo, G., and Joseph, E.: A trajectory-based estimate of the tropospheric ozone column using the residual method, J. Geophys. Res., 112, D24S49, doi:10.1029/2007JD008773, 2007.
Stajner, I., Wargan, K., and Pawson, S.: Assimilated ozone from EOS-Aura: evaluation of the tropopause region and tropospheric columns, J. Geophys. Res., 113, D16S32, doi:10.1029/2007JD008863, 2008.
Tan, W. W., Geller, M. A., Pawson, S., and da Silva, A.: A case study of excessive subtropical transport in the stratosphere of a data assimilation system, J. Geophys. Res., 109, D11102, doi:10.1029/2003JD004057, 2004.
Waters, J. W., Froidevaux, L., Harwood, R. S., Jarnot, R. F., Pickett, H. M., Read, W. G., Siegel,

ACPD
11, 17879–17911, 2011

P. H., Cofield, R. E., Filipiak, M. J., Flower, D. A., Holden, J. R., Lau, G. K., Livesey, N. J., Manney, G. L., Pumphrey, H. C., Santee, M. L., Wu, D. L., Cuddy, D. T., Lay, R. R., Loo, M. S., Perun, V. S., Schwartz, M. J., Stek, P. C., Thurstans, R. P., Boyles, M. A., Chandra, S., Chavez, M. C., Chen, G.-S., Chudasama, B. V., Dodge, R., Fuller, R. A., Girard, M. A., Jiang, J. H., Jiang, Y., Knosp, B. W., LaBelle, R. C., Lam, J. C., Lee, K. A., Miller, D., Oswald, J. E., Patel, N. C., Pukala, D. M., Quintero, O., Scaff, D. M., Snyder, W. V., Tope, M. C., Wagner, P. A., and Walch, M. J.: The Earth Observing System Microwave Limb Sounder (EOS MLS) on the Aura satellite, IEEE T. Geophys. Remote, 44(5), 1075–1092, 2006.

Zhang, L., Jacob, D. J., Liu, X., Logan, J. A., Chance, K., Eldering, A., and Bojkov, B. R.: Intercomparison methods for satellite measurements of atmospheric composition: application to tropospheric ozone from TES and OMI, Atmos. Chem. Phys., 10, 4725–4739, doi:10.5194/acp-10-4725-2010, 2010.

Ziemke, J. R., Chandra, S., Duncan, B. N., Froidevaux, L., Bhartia, P. K., Levelt, P. F., and Waters, J. W.: Tropospheric ozone determined from Aura OMI and MLS: evaluation of measurements and comparison with the Global Modeling Initiative's Chemical Transport Model, J. Geophys. Res., 111, D19303, doi:10.1029/2006JD007089, 2006.

ACPD
11, 17879–17911, 2011

Table 1. Statistical comparisons between OMI/MLS and SHADOZ/WOUDC sonde tropospheric mean volume mixing ratio (in ppbv) with the station latitudes arranged from northernmost at top to southern-most at bottom. Included for each station is the total number of daily profile measurements, mean values for OMI/MLS and ozonesondes, and standard RMS of their differences.

Station	*N*	OMI/MLS	Sonde	Diff RMS
Alert (82.5° N, 62.3° W)	27	60.2	49.4	19.4
Eureka (80.0° N, 85.9° W)	22	56.9	50.5	13.3
Resolute (74.7° N, 95.0° W)	33	61.9	49.7	19.1
Neumayer (70.7° S, 8.3° W)	26	38.4	30.8	17.7
Lerwick (60.1° N, 1.2° W)	46	57.2	55.2	10.7
Churchill (58.7° N, 94.1° W)	36	61.1	50.6	14.3
Stonyplain (53.6° N, 114.1° W)	45	53.1	48.2	11.0
Goosebay (53.3° N, 60.4° W)	38	57.9	51.4	13.2
Legionwo (52.4° N,21.0° E)	39	51.8	56.5	12.1
Lindenberg (52.2° N, 14.1° E)	48	51.0	55.9	11.1
Debilt (52.1° N, 5.2° E)	45	52.1	54.7	8.4
Valentia (51.9° N, 10.3° W)	27	56.0	58.0	9.4
Brattslake (50.2° N, 104.7° W)	46	51.9	51.4	12.3
Praha (50.0° N, 14.5° E)	12	50.4	54.1	7.9
Kelowna (49.9° N, 119.4° W)	36	51.1	51.8	12.4
Payerne (46.8° N, 7.0° E)	48	51.7	52.2	6.6
Egbert (44.2° N, 79.8° W)	41	58.3	57.8	9.3
Barajas (40.5° N, 3.6° W)	47	55.9	53.9	7.0
Boulder (40.3° N, 105.2° W)	36	54.0	56.0	6.6
Ankara (40.0° N, 32.9° E)	43	57.5	59.2	9.9
Wallops (37.9° N, 75.5° W)	48	58.6	59.2	6.9
Huntsville (34.7° N, 86.6° W)	36	56.3	52.6	12.4
Isfahan (32.5° N, 51.7° E)	29	61.1	61.3	11.5
Hongkong (22.3° N, 114.2° E)	47	49.7	50.9	7.8
Hilo (19.4° N, 155.0° W)	58	46.3	50.9	6.8
Alajuela (10.0° N, 84.2° W)	27	40.7	40.5	4.2
Heredia (10.0° N, 84.1° W)	16	40.7	43.5	5.9
Panama (7.8° N, 80.3° W)	2	38.7	44.0	6.5
Kuala (2.7° N, 101.7° E)	51	34.2	35.2	5.6
Sancr (0.9° S, 89.6° W)	31	38.4	36.7	5.0
Nairobi (1.3° S, 36.8° E)	52	37.8	46.2	9.9
Malindi (3.0° S, 40.2° E)	13	45.0	51.3	7.6
Natal (5.4° S, 35.4° W)	58	47.7	49.0	6.0
Java (7.5° S, 112.6° E)	44	35.3	34.8	6.7
Ascen (8.0° S, 14.4° W)	56	50.9	55.2	6.7
Samoa (14.2° S, 170.6° W)	56	31.5	30.8	4.5
Fiji (18.1° S, 178.4° E)	22	34.7	34.2	4.7
Reunion (21.0° S, 55.5° E)	52	50.5	59.9	11.7

ACPD
11, 17879–17911, 2011

Table 2. Tropospheric column ozone zonal mean climatology (in Dobson Units) from OMI/MLS at 5° latitude resolution.

Latitudes	Jan	Feb	Mar	Apr	May	Jun	Jul	Aug	Sep	Oct	Nov	Dec
60–65° N	35.8	34.6	33.1	33.7	34.3	33.8	33.8	30.7	28.2	27.9	33.8	35.8
55–60° N	33.0	32.2	33.0	33.7	34.6	35.6	35.5	32.9	29.5	28.1	30.3	33.6
50–55° N	31.1	32.1	32.9	33.5	35.2	36.7	36.9	34.7	30.8	28.4	28.8	30.1
45–50° N	29.4	30.8	31.6	33.7	35.9	38.2	39.1	37.4	33.2	28.9	27.9	28.0
40–45° N	27.6	28.9	30.9	34.1	37.0	40.9	42.2	40.7	35.7	30.2	27.3	27.3
35–40° N	27.0	27.7	30.9	35.2	38.9	43.0	44.0	42.3	37.9	32.4	28.4	27.3
30–35° N	28.2	28.6	32.9	38.0	41.2	42.9	42.3	40.4	37.3	33.5	30.9	29.0
25–30° N	30.2	31.6	35.9	40.5	42.0	39.8	38.3	36.8	35.0	33.1	31.9	30.6
20–25° N	31.6	32.4	36.9	40.5	40.4	37.1	35.3	33.6	33.0	32.0	31.7	31.6
15–20° N	31.1	31.3	35.2	38.0	37.1	34.3	32.0	30.0	29.8	29.7	30.2	31.0
10–15° N	29.2	29.3	32.7	34.1	32.6	30.3	28.2	26.8	27.3	27.7	28.6	29.5
5–10° N	27.2	27.6	29.9	29.8	27.7	26.5	25.8	25.1	26.1	26.3	26.6	27.7
0–5° N	25.2	25.5	26.8	26.0	24.9	25.3	25.8	26.4	27.2	26.9	26.4	26.4
0–5° S	24.4	24.0	24.8	24.1	25.0	26.9	27.5	28.7	30.1	29.9	28.5	26.9
5–10° S	24.2	22.9	23.4	23.5	25.4	27.8	28.5	30.0	32.0	32.3	30.4	27.7
10–15° S	24.5	23.0	23.6	23.9	26.0	28.7	29.5	30.8	33.3	33.9	32.1	28.7
15–20° S	26.6	24.7	24.8	25.2	27.1	29.8	31.0	32.5	35.5	36.4	34.2	30.5
20–25° S	29.8	27.9	27.6	27.6	28.7	30.9	32.7	35.1	38.2	39.5	37.3	33.5
25–30° S	32.4	30.6	29.9	29.3	29.8	31.4	34.2	36.8	40.2	41.2	39.3	36.2
30–35° S	33.9	31.8	30.5	28.6	28.3	30.0	33.4	36.2	38.9	39.5	37.5	35.9
35–40° S	32.2	30.4	28.4	26.4	26.2	27.6	30.7	33.9	35.4	35.0	32.5	31.7
40–45° S	28.0	27.2	26.0	25.6	25.6	26.5	28.5	30.5	31.6	30.3	28.3	27.1
45–50° S	25.6	25.8	25.7	25.9	25.8	25.9	26.7	28.2	30.6	29.9	28.0	25.8
50–55° S	25.3	26.5	27.8	27.5	27.8	29.7	28.5	28.0	31.4	30.7	28.4	25.4
55–60° S	23.6	26.5	28.4	26.8	28.6	28.5	29.4	28.8	30.2	29.5	26.7	23.7
60–65° S	22.6	25.8	27.5	26.6	29.8	33.2	33.6	28.3	27.0	31.2	25.8	22.0

ACPD
11, 17879–17911, 2011

Table 3. Global stratospheric column ozone zonal mean climatology (in Dobson Units) derived from MLS integrated ozone profiles at 5° latitude resolution.

Latitudes	Jan	Feb	Mar	Apr	May	Jun	Jul	Aug	Sep	Oct	Nov	Dec
85–90° N	311	350	352	340	324	297	269	253	243	246	267	279
80–85° N	314	363	361	359	330	300	269	252	244	251	270	281
75–80° N	319	363	363	359	330	301	272	254	248	254	275	287
70–75° N	326	359	361	359	333	303	275	262	256	259	279	293
65–70° N	330	359	359	355	332	304	280	269	262	265	280	299
60–65° N	333	359	359	352	331	306	286	274	267	269	283	306
55–60° N	332	355	354	347	329	307	291	277	270	270	282	309
50–55° N	329	349	348	340	325	306	290	276	267	267	279	308
45–50° N	321	338	338	331	318	299	280	269	262	260	273	302
40–45° N	307	320	324	318	304	286	266	259	254	252	265	289
35–40° N	284	292	300	298	286	271	256	252	248	243	252	269
30–35° N	257	262	272	275	269	259	251	248	244	237	237	247
25–30° N	234	238	248	255	256	252	248	246	242	234	229	230
20–25° N	221	224	234	242	246	246	245	244	240	232	224	219
15–20° N	215	218	227	235	240	242	244	245	241	232	223	215
10–15° N	214	216	224	232	237	240	244	245	242	232	223	214
5–10° N	215	217	223	230	234	237	240	242	240	231	224	216
0–5° N	219	221	226	231	232	233	236	238	237	229	225	219
0–5° S	223	224	228	231	230	229	230	233	233	228	225	222
5–10° S	225	226	228	229	227	224	225	228	230	228	227	225
10–15° S	227	227	227	227	223	221	223	226	230	229	230	228
15–20° S	228	226	226	225	222	222	225	228	234	234	233	230
20–25° S	228	225	225	225	224	226	230	235	242	241	239	232
25–30° S	229	226	227	228	229	234	239	248	254	251	247	237
30–35° S	232	230	231	233	239	249	255	267	271	267	259	243
35–40° S	238	235	236	240	250	265	275	288	292	287	274	252
40–45° S	248	242	241	247	259	276	290	303	308	304	288	263
45–50° S	260	250	247	255	267	282	298	310	316	313	298	273
50–55° S	269	257	252	259	270	282	294	305	314	313	302	280
55–60° S	275	262	257	262	271	278	281	284	290	299	299	283
60–65° S	274	264	258	261	269	273	264	247	242	271	283	280
65–70° S	269	261	257	256	263	264	247	211	186	233	254	273
70–75° S	264	257	257	250	254	253	235	198	150	196	224	267
75–80° S	259	253	252	242	247	244	226	196	135	173	205	260
80–85° S	258	252	246	237	238	237	225	202	134	147	190	256
85–90° S	252	246	237	230	237	236	225	204	135	142	187	252

ACPD
11, 17879–17911, 2011

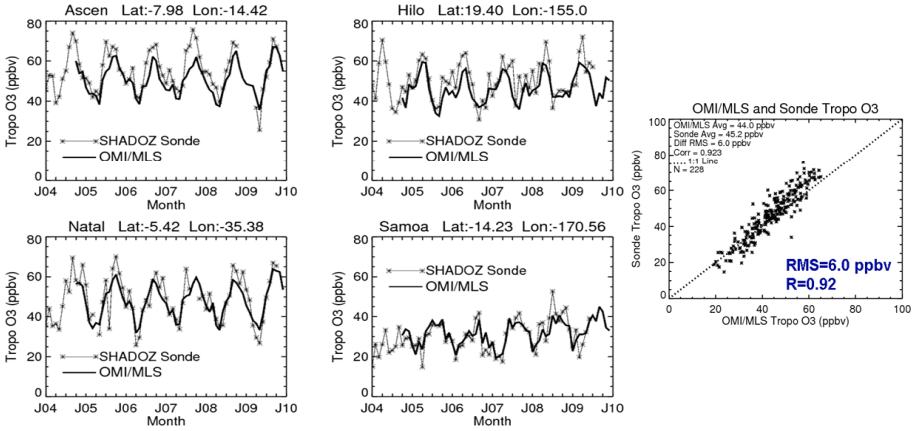

Fig. 1. Comparison time series of tropospheric ozone mean volume mixing ratio (in ppbv) between OMI/MLS (dark curves) and several selected common station measurements from SHADOZ (light curves). Also included at far right is a 1-1 comparison scatter plot for the measurements.

ACPD
11, 17879–17911, 2011

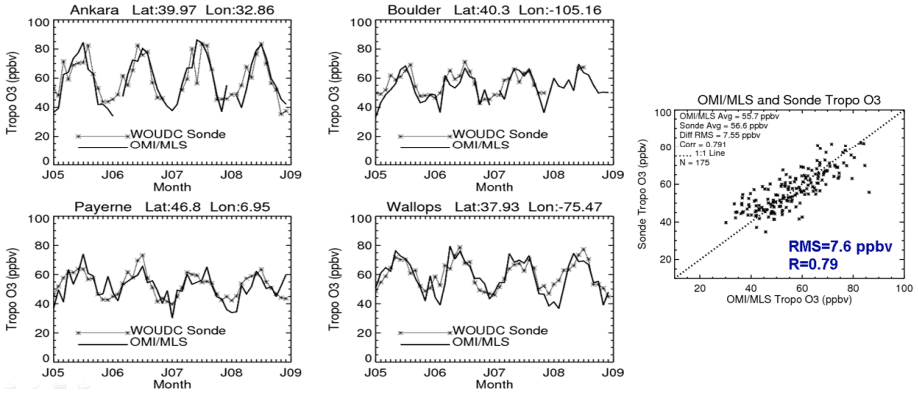

Fig. 2. Similar to Fig. 1 but for selected extra-tropical WOUDC ozonesonde stations.

ACPD
11, 17879–17911, 2011

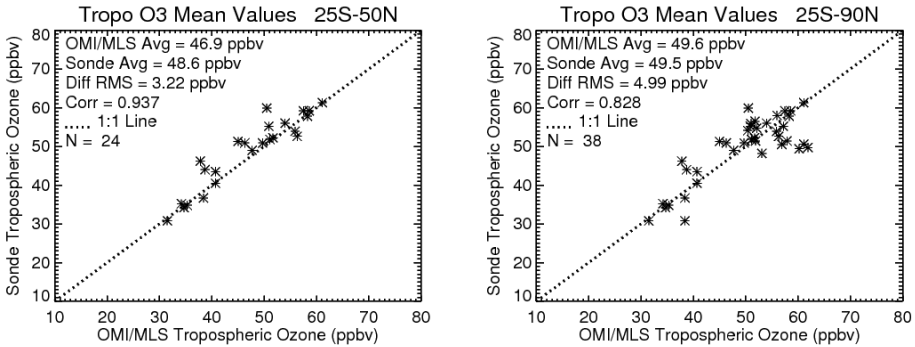

Fig. 3. (left) Scatter plots of ozonesonde versus OMI/MLS mean tropospheric ozone for ozonesonde station locations lying between 25° S and 50° N. (right) Same as left panel, except for extended latitude range 25° S to 90° N. The values plotted are time series averages in units ppbv.

ACPD
11, 17879–17911, 2011

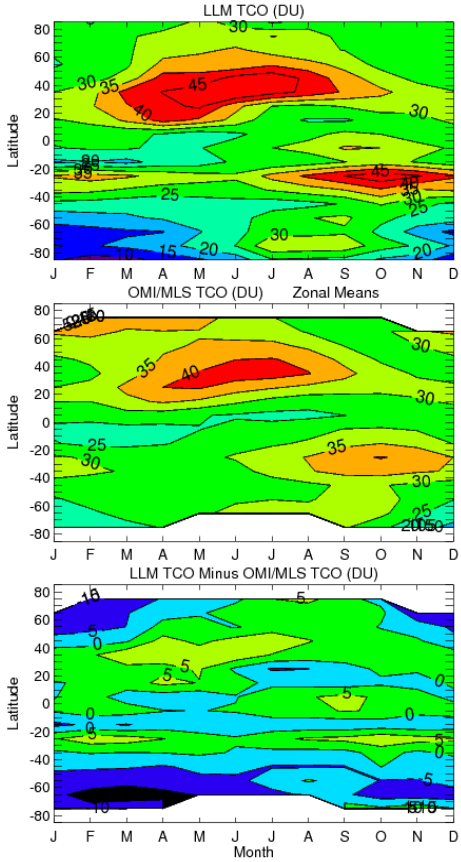

Fig. 4. (top) Labow-Logan_McPeters (LLM) tropospheric column ozone climatology. (middle) OMI/MLS tropospheric column ozone climatology. (bottom) LLM minus OMI/MLS climatology difference. All measurements are in Dobson Units. The colors in the panels going from blue/black to red represent smallest to largest (or most positive) values, respectively.

ACPD
11, 17879–17911, 2011

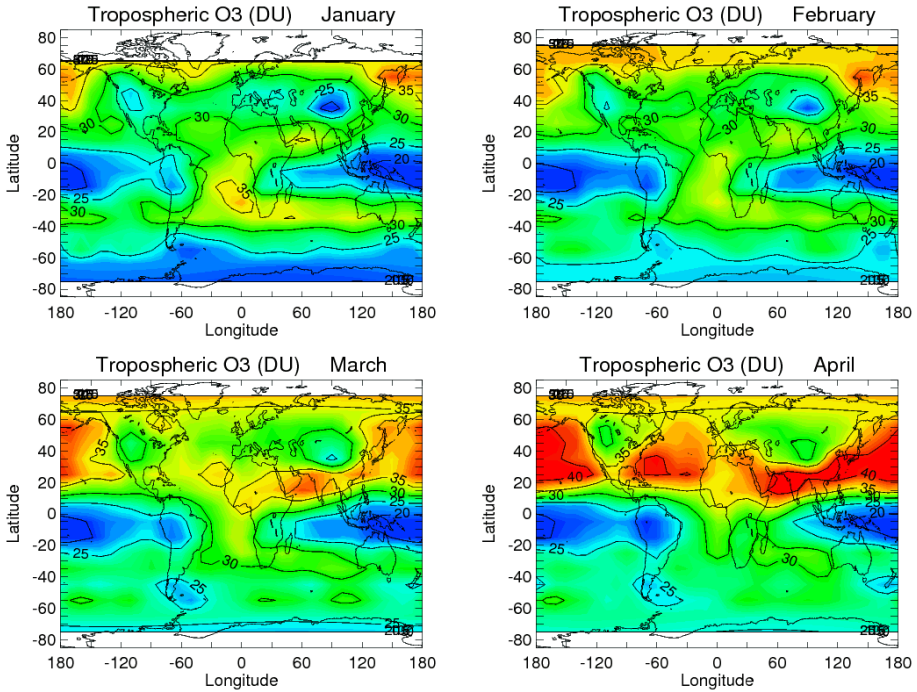

Fig. 5a. Tropospheric column ozone climatology (in Dobson Units) for months January–April from OMI/MLS residual ozone measurements. The colors in the panels going from blue to red represent smallest to largest values, respectively.

ACPD
11, 17879–17911, 2011

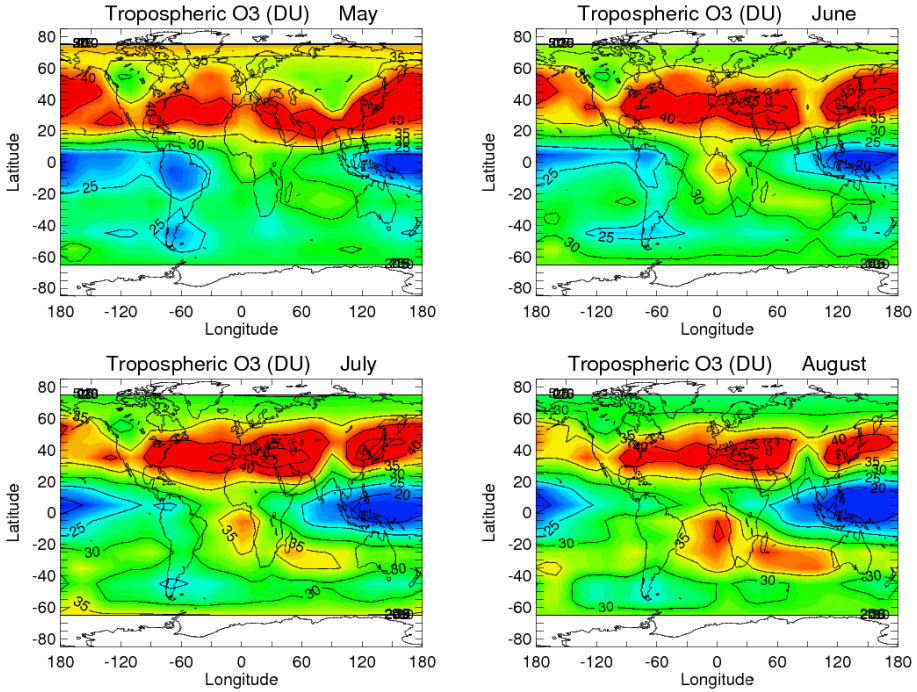

Fig. 5b. Same as Fig. 5a but for months May–August.

ACPD
11, 17879–17911, 2011

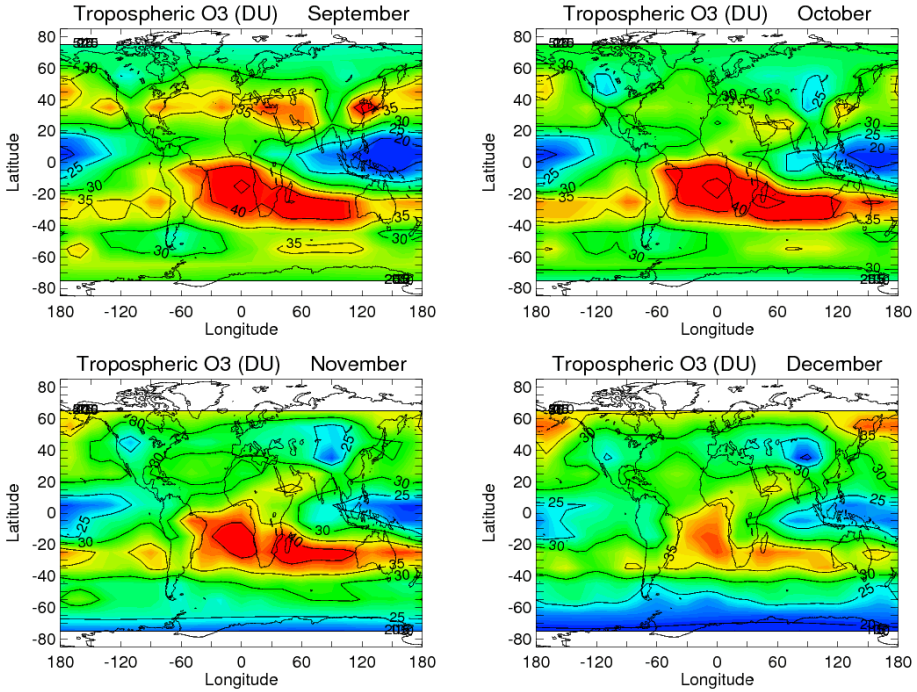

Fig. 5c. Same as Fig. 5b but for months September–December.

ACPD
11, 17879–17911, 2011

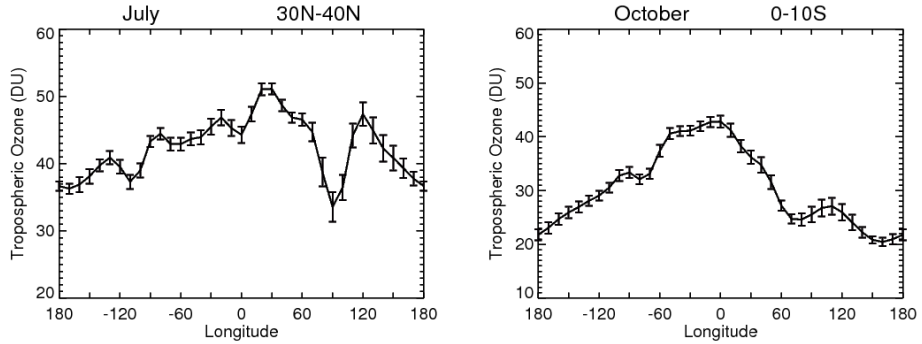

Fig. 6. Line plots of tropospheric column ozone (in Dobson Units) as a function of longitude for the latitude bands 30°–40° N and 0°–10° S. The plots include $\pm 2\sigma$ uncertainties for illustration where σ is the calculated standard RMS error of the mean.

ACPD
11, 17879–17911, 2011

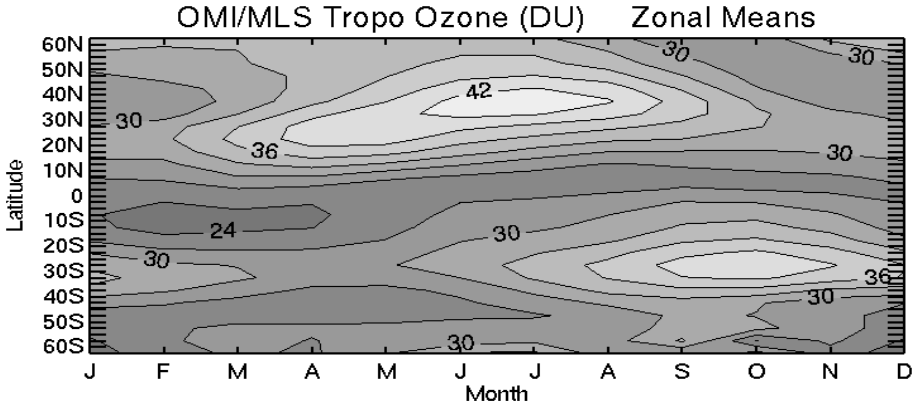

Fig. 7. Zonal mean climatology of tropospheric column ozone (in Dobson Units) derived from October 2004–December 2010 OMI/MLS at 5° latitude resolution. The shading going from dark to light represents smallest to largest values, respectively.

ACPD
11, 17879–17911, 2011

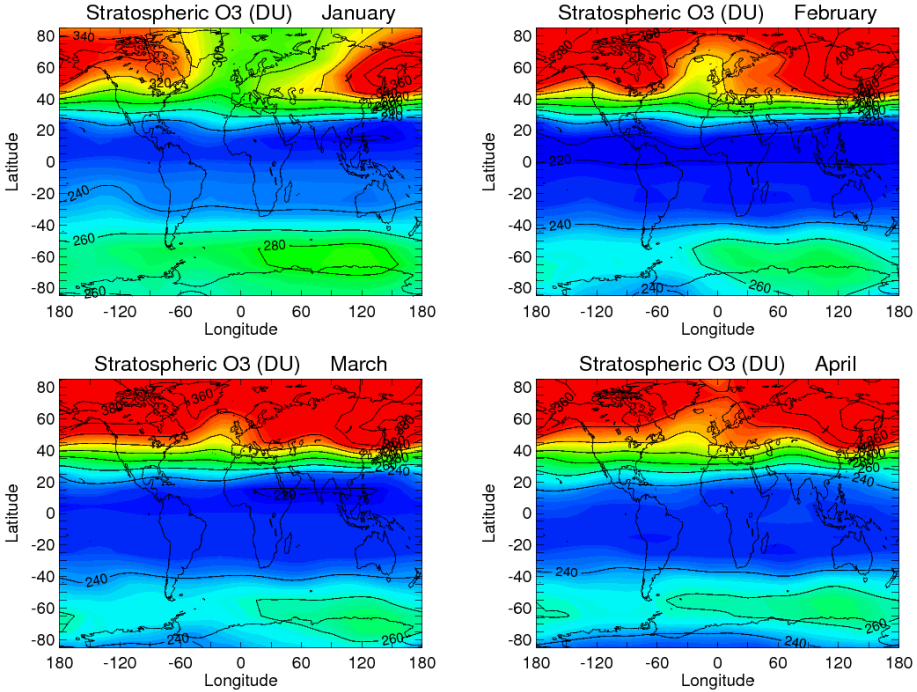

Fig. 8a. Similar to Fig. 5a but for stratospheric column ozone (in Dobson Units). The colors in the panels going from blue to red represent smallest to largest values, respectively.

ACPD
11, 17879–17911, 2011

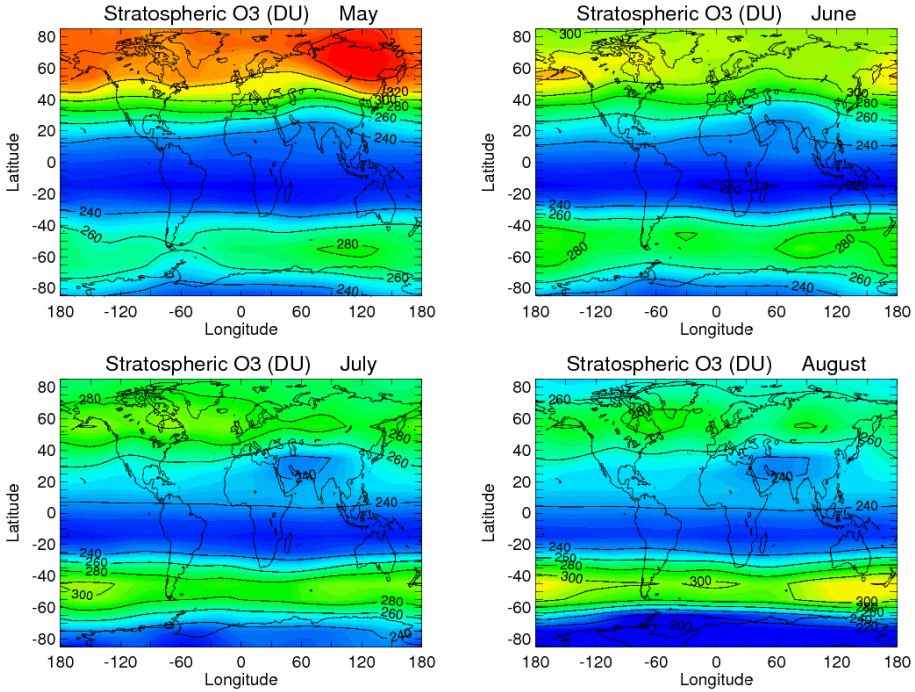

Fig. 8b. Similar to Fig. 5b but for stratospheric column ozone (in Dobson Units).

ACPD
11, 17879–17911, 2011

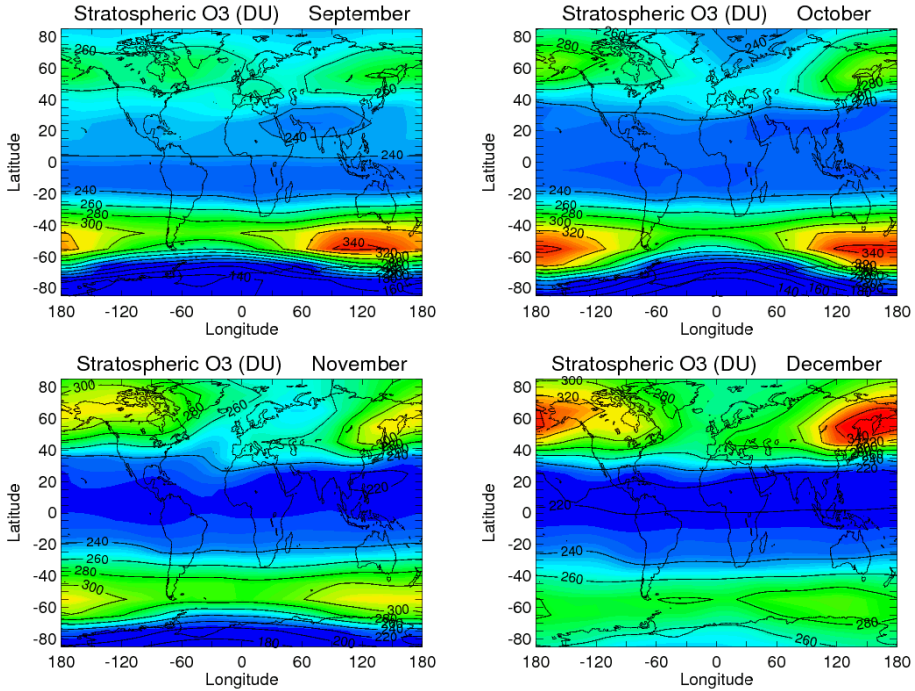

Fig. 8c. Similar to Fig. 5c but for stratospheric column ozone (in Dobson Units).

ACPD
11, 17879–17911, 2011

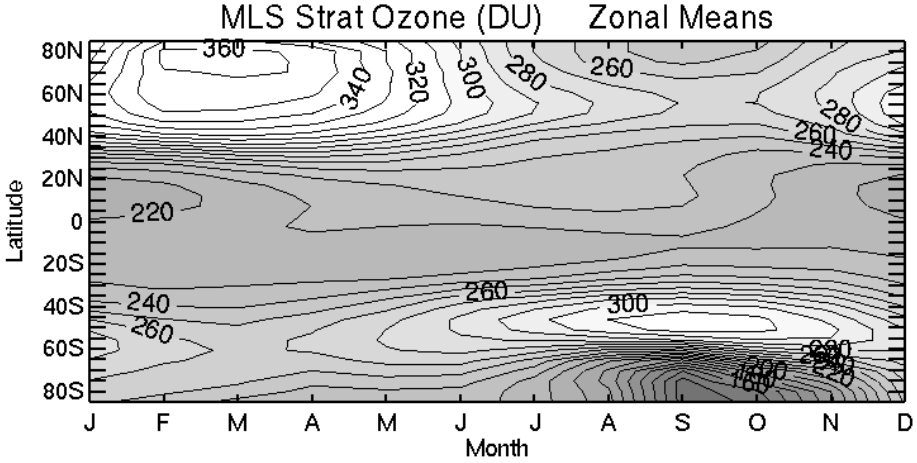

Fig. 9. Zonal mean climatology of stratospheric column ozone (in Dobson Units) from October 2004–December 2010 MLS at 5° latitude resolution. The shading going from dark to light represents smallest to largest values, respectively.

ACPD
11, 17879–17911, 2011